heat maps, such as those displayed in Fig. 4, can suggest optimal targets. For example, node C is not only highly influential, highly susceptible, and has peers who are themselves influential and susceptible, but is also of above average degree in its region and has many peers who are susceptible rather than one highly susceptible peer driving the average susceptibility in its network. These characteristics in combination make C a good target.

Our method uses randomized experiments to identify influential and susceptible individuals in large social networks; however, the work does have limitations. Although we avoid bias by randomizing message recipient selection and holding message content constant, recipient selection and message content may be important aspects of influence and should therefore be estimated in future experiments. Furthermore, it is still not clear whether influence and susceptibility are generalized characteristics of individuals or instead depend on which product, behavior, or idea is diffusing. Although our estimates should generalize to the diffusion of similar products, they are not conclusions about who is more or less influential in general. Our experimental methods for influence identification, however, are generalizable and can be used to measure influence and susceptibility in the diffusion of other products and behaviors in a variety of settings.

Previous research has taken an individualistic view of influence—that someone's importance to the diffusion of a behavior depends only on his or her individual attributes or personal network characteristics. In contrast, our results show that the joint distributions of influence, susceptibility, and the likelihood of spontaneous adoption in the local network around individuals together determine their importance to the propagation of behaviors. Future research should therefore examine how the codistribution of influence, susceptibility, and dyadic induction in networks affects the diffusion of behaviors, the development of social contagions, and the effects of policies intended to promote or contain behavior change. More generally, our results show the potential of methods based on large-scale in vivo randomized experiments to robustly estimate peer effects and identify influential and susceptible members of social networks.

References and Notes

1. S. Aral, *Mark. Sci.* **30**, 217 (2011).
2. S. Aral, D. Walker, *IEEE Intell. Syst.* **26**, 91 (2011).
3. G. Kossinets, D. J. Watts, *Science* **311**, 88 (2006).
4. D. Lazer *et al.*, *Science* **323**, 721 (2009).
5. N. Eagle, M. Macy, R. Claxton, *Science* **328**, 1029 (2010).
6. S. A. Golder, M. W. Macy, *Science* **333**, 1878 (2011).
7. S. Aral, M. W. Van Alstyne, *Am. J. Sociol.* **117**, 90 (2011).
8. E. Sun, I. Rosenn, C. Marlow, T. Lento, in *Proceedings of the Third International Conference on Weblogs and Social Media* (AAAI Press, Menlo Park, CA, 2009).
9. J. Leskovec, L. A. Adamic, B. A. Huberman, *ACM Trans. Web* 10.1145/1232722.1232727 (2007).
10. M. McPherson, L. Smith-Lovin, J. M. Cook, *Annu. Rev. Sociol.* **27**, 415 (2001).
11. S. Aral, L. Muchnik, A. Sundararajan, *Proc. Natl. Acad. Sci. U.S.A.* **106**, 21544 (2009).
12. C. F. Manski, *Soc. Methodol.* **23**, 1 (1993).
13. S. Currarini, M. O. Jackson, P. Pin, *Proc. Natl. Acad. Sci. U.S.A.* **107**, 4857 (2010).
14. H. Noel, B. Nyhan, *Soc. Networks* **33**, 211 (2011).
15. W. Hartmann *et al.*, *Mark. Lett.* **19**, 287 (2008).
16. N. A. Christakis, J. H. Fowler, *N. Engl. J. Med.* **357**, 370 (2007).
17. R. Lyons, *Stat. Polit. Policy* 10.2202/2151-7509.1024 (2011).
18. C. R. Shalizi, A. C. Thomas, *Sociol. Methods Res.* **40**, 211 (2011).
19. S. Aral, D. Walker, *Manage. Sci.* **57**, 1623 (2011).
20. D. Centola, *Science* **329**, 1194 (2010).
21. S. Leider, M. M. Möbius, T. Rosenblat, Q.-A. Do, *Q. J. Econ.* **124**, 1815 (2009).
22. E. Bakshy, I. Rosenn, C. Marlow, L. Adamic, in *WWW '12 Proceedings of the 21st International Conference on World Wide Web* (ACM, New York, 2012), pp. 519–528.
23. E. Katz, *Public Opin. Q.* **21**, 61 (1957).
24. T. W. Valente, *Network Models of the Diffusion of Innovations* (Hampton, Cresskill, NJ, 1995).
25. D. Kempe, J. Kleinberg, É. Tardos, in *Proceedings of the Ninth ACM SIGKDD International Conference on Knowledge Discovery and Data Mining* (Association for Computing Machinery, New York, 2003), pp. 137–146.
26. M. Granovetter, *Am. J. Sociol.* **83**, 1420 (1978).
27. D. J. Watts, P. S. Dodds, *J. Consum. Res.* **34**, 441 (2007).
28. P. S. Dodds, D. J. Watts, *Phys. Rev. Lett.* **92**, 218701 (2004).
29. D. Centola, M. Macy, *Am. J. Sociol.* **113**, 702 (2007).
30. D. Godes *et al.*, *Mark. Lett.* **16**, 415 (2005).
31. C. Heath, C. Bell, E. Sternberg, *J. Pers. Soc. Psychol.* **81**, 1028 (2001).
32. R. Iyengar, C. Van den Bulte, T. W. Valente, *Marketing Sci.* **30**, 195 (2011).

Acknowledgments: We thank S. Aral, H. Frydman, C. Hurvich, P. Perry, J. Simonoff, and M. Sternberg for invaluable discussions. Supported by a Microsoft research faculty fellowship (S.A.) and by NSF Career Award 0953832 (S.A.). The research was approved by the NYU institutional review board. There are legal obstacles to making the data available, but code is available upon request. The requests for data and randomization of message targets we used are standard ways in which applications request and use user data on Facebook. They are covered by the Facebook privacy policy and terms of service. Opt-in permissions were granted by the user to the application developer on a per-application basis when the user installed the application, via Facebook application authentication dialogs. In the dialogs we asked for all the categories of data we used in the study, and all of these requests were in line with the Facebook terms of service. Users saw these requests and opted in to them before installing the app.

Supplementary Materials

www.sciencemag.org/cgi/content/full/science.1215842/DC1
Materials and Methods
Figs. S1 to S12
Tables S1 to S9

26 October 2011; accepted 30 May 2012
Published online 21 June 2012;
10.1126/science.1215842

Sex-Specific Adaptation Drives Early Sex Chromosome Evolution in *Drosophila*

Qi Zhou and Doris Bachtrog*

Most species' sex chromosomes are derived from ancient autosomes and show few signatures of their origins. We studied the sex chromosomes of *Drosophila miranda*, where a neo-Y chromosome originated only approximately 1 million years ago. Whole-genome and transcriptome analysis reveals massive degeneration of the neo-Y, that male-beneficial genes on the neo-Y are more likely to undergo accelerated protein evolution, and that neo-Y genes evolve biased expression toward male-specific tissues—the shrinking gene content of the neo-Y becomes masculinized. In contrast, although older X chromosomes show a paucity of genes expressed in male tissues, neo-X genes highly expressed in male-specific tissues undergo increased rates of protein evolution if haploid in males. Thus, the response to sex-specific selection can shift at different stages of X differentiation, resulting in masculinization or demasculinization of the X-chromosomal gene content.

X and Y chromosomes follow distinctive evolutionary trajectories after recombination becomes suppressed between ancestral homologous autosomes with a sex-determining function (*1*). The lack of recombination greatly impairs natural selection on the Y, which loses most of its original genes and often accumulates repetitive DNA (*2*). However, Y chromosomes are not complete evolutionary dead ends; instead, their male-limited transmission favors the gain of male-related genes ("masculinization"). Low gene density yet enrichment of male-specific genes is shared among many independently evolved ancient Ys (*3*, *4*), but few traces of their evolutionary origins remain, making processes involved in Y degeneration little understood. Conversely, the X still recombines in females, and selection can effectively purge deleterious alleles and incorporate beneficial mutations (*2*). Unlike autosomes, the X is transmitted more often through females than males, favoring an underrepresentation of male-beneficial genes on the X ("demasculinization") (*5*, *6*). Further, almost all X-linked genes are haploid in males (hemizygous) and can fix re-

Department of Integrative Biology, University of California Berkeley, Berkeley, CA 94720, USA.

*To whom correspondence should be addressed. E-mail: dbachtrog@berkeley.edu

cessive male-advantageous alleles more easily than can autosomes (*7*), potentially leading to masculinization. These aspects of X chromosome biology dictate unusual and sometimes opposing patterns of sequence and expression evolution (*8*) but are difficult to distinguish in ancestral systems.

The genome of *Drosophila* fly species can be divided into a set of homologous chromosomal arms called "Muller elements" (*9*). Chromosomal fusions between the ancient sex chromosomes (Muller-A element, referred here as "chrXL" and "chrY") with autosomes have repeatedly generated younger secondary sex chromosomes. Male *Drosophila* lack meiotic recombination (*9*); thus, Y-fused autosomes (neo-Ys) cannot recombine with their homologs (neo-Xs), which sets the stage for sex chromosome differentiation. *D. miranda* harbors two such successive fusions that created sex chromosomes of different ages (Fig. 1A) (*10*). Muller-D became sex-linked before the divergence of *D. miranda* and *D. pseudoobscura* roughly 10 to 18 million years ago and resembles the ancestral sex chromosomes; the non-recombining Muller-D element is almost completely degenerated and now part of the heterochromatic Y (*11*), whereas its recombining counterpart ("chrXR") evolved an architecture typical of an X (*5*, *12*). Another fusion specific to *D. miranda* involves Muller-C element (referred as "neo-X" and "neo-Y") and occurred only about 1 million years ago (*13*). This very young sex-chromosome system is in the process of evolving from a pair of ordinary autosomes to a pair of heteromorphic sex chromosomes. Cytogenetic studies and investigations of individual genes or genomic regions have revealed that the *D. miranda* neo-Y is intermediately degenerate (*10*, *14*–*16*), rendering the neo-X partially hemizygous.

We conducted a whole-genome analysis of the neo-sex chromosomes, integrated with transcriptomes from multiple tissues using next-generation sequencing technology. We sequenced both sexes of an inbred *D. miranda* strain (MSH22), and assembled scaffolds were anchored onto the *D. pseudoobscura* genome (table S1) (*17*). We annotated a total of 14,819 proteins for the *D. miranda* genome, using 16,133 *D. pseudoobscura* proteins as queries. We assessed the quality of our assemblies using bacterial artificial chromosome clone sequences and 454 data (table S3) and validated our chromosomal assignments by comparing male and female mapping coverage along each chromosome (Fig. 1B). Coverage of male and female coincides well along the autosomes, whereas both chrXL and chrXR show only about half as many reads mapped in males as in females (Fig. 1B and table S4), indicating that their homologous ancient Ys are too degenerate to show any significant sequence similarity. In contrast, male coverage along the neo-X is about three quarters that of females, suggesting that parts of the neo-Y are highly diverged from the neo-X. Of the neo-X sequence, 71.8% can be aligned with the neo-Y, with 1.5% (±0.00093%) nucleotide divergence between aligned regions. Coding regions are under stronger selective constraint and exhibit a higher alignment rate (92.6%) and lower divergence between the neo-X and neo-Y (1.1% ± 0.18%).

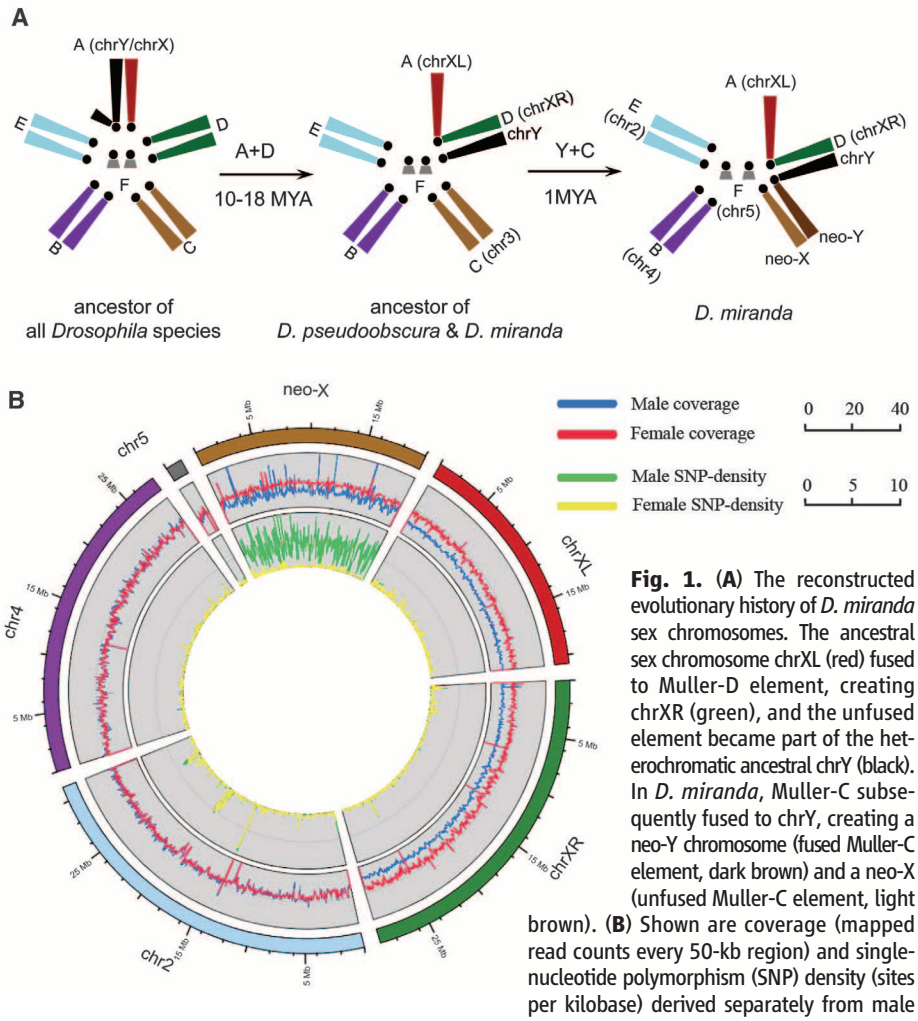

Fig. 1. (**A**) The reconstructed evolutionary history of *D. miranda* sex chromosomes. The ancestral sex chromosome chrXL (red) fused to Muller-D element, creating chrXR (green), and the unfused element became part of the heterochromatic ancestral chrY (black). In *D. miranda*, Muller-C subsequently fused to chrY, creating a neo-Y chromosome (fused Muller-C element, dark brown) and a neo-X (unfused Muller-C element, light brown). (**B**) Shown are coverage (mapped read counts every 50-kb region) and single-nucleotide polymorphism (SNP) density (sites per kilobase) derived separately from male and female genomic reads in a 5-kb sliding window across the *D. miranda* genome. The high male SNP density along the neo-X (male, 3.696 versus female, 0.080 sites per kilobase) reflects divergence between the neo-X and neo-Y chromosomes.

We compared protein-coding regions to gain insights into the process of gene loss of a Y. The neo-X and neo-Y are derived from a gene-rich autosome, with initially identical gene sets (*10*): 2951 genes with intact open reading frames (ORFs) could be annotated on the neo-X, whereas only 1941 intact ORFs were identified on the neo-Y. The remaining 1010 genes that were ancestrally present on the neo-Y (34.2%) are probably nonfunctional: 848 ORFs are disrupted by premature terminal codons (PTC) and/or frame-shift mutations, and 162 genes are partially or completely deleted from the neo-Y (Fig. 2A) (*17*). No spatial clustering of nonfunctional genes was detected on the neo-Y (Fig. 2B).

Severely disabling mutations have also accumulated in regulatory regions on the neo-Y. We compared allelic expression of 2165 neo-sex linked genes in males that were expressed from the neo-X: 883 genes (40.8%) show similar levels of expression from both chromosomes, whereas 947 (43.7%) are expressed at a significantly higher level from the neo-X, and 335 genes (15.5%) are neo-Y–biased (binomial test, $P < 0.05$), whereas 220 genes (10.2%) with a transcribed neo-X copy are completely silenced on the neo-Y. A large fraction of neo-Y genes is still transcribed, despite having disrupted ORFs: 83.0% of all neo-Y genes with nonsense mutations are transcribed, yet at a significantly lower level than that of genes with intact neo-Y ORFs (Wilcoxon test, $P < 2.2 \times 10^{-16}$) (Fig. 2B). This implies that down-regulated genes either tend to acquire nonsense mutations or that pseudogenes become transcriptionally silenced on the neo-Y but could also reflect up-regulation of the neo-X copy at nonfunctional neo-Y genes (dosage compensation) (*12*). Gene loss is nonrandom with regard to gene function. Nonfunctional and down-regulated genes on the neo-Y are significantly enriched for

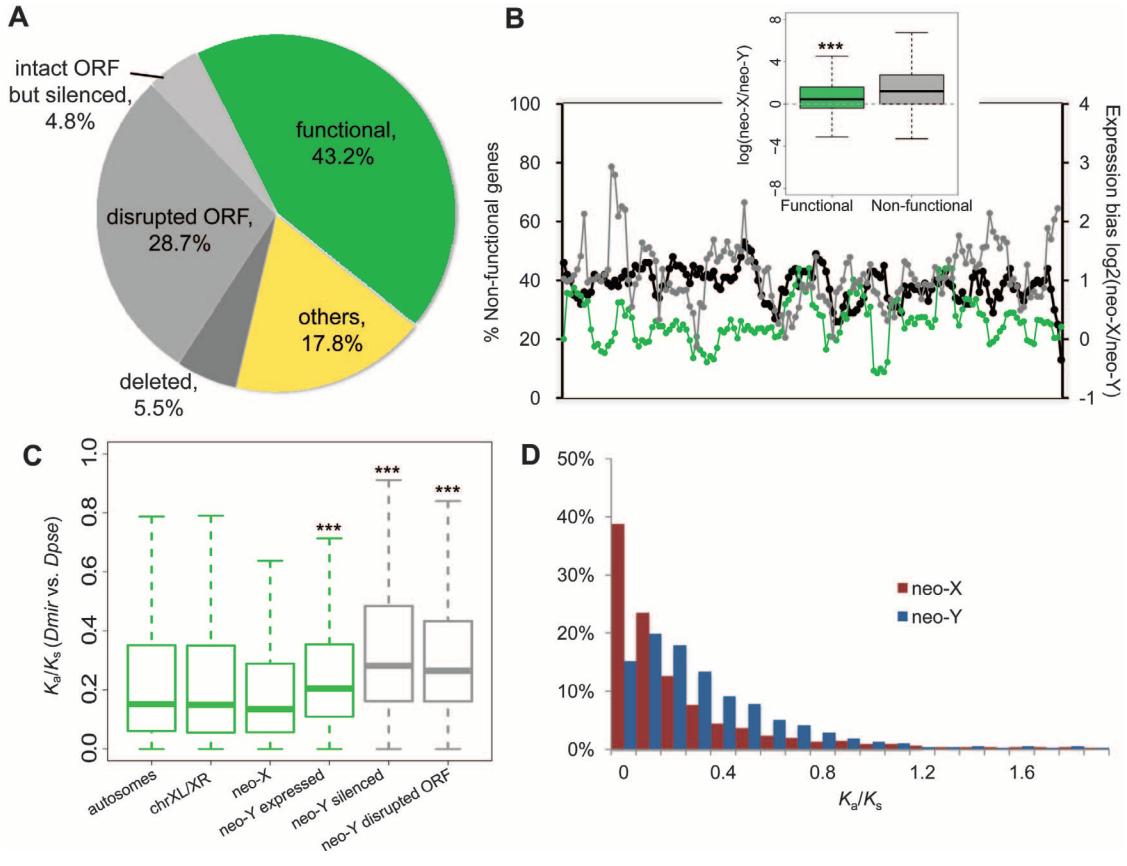

Fig. 2. (**A**) Composition of neo-Y genes with regard to inferred functionality (green, intact ORFs and detectable expression in adult male; gray, disrupted ORF and/or silenced expression; and yellow, genes without neo-X expression or without diagnostic SNPs). (**B**) The chromosomal distribution of nonfunctional genes across a sliding window size of 20 genes (black line). Average neo-X expression bias within the investigated window was calculated from log ratios of neo-X versus neo-Y expression for functional (green) and nonfunctional (gray) genes. Functional neo-Y genes show significantly less neo-X–biased expression than do nonfunctional genes (boxplot, $P < 2.2 \times 10^{-16}$, Wilcoxon test). (**C**) Evolutionary rate comparisons (K_a/K_s ratios relative to *D. pseudoobscura*) among genes on different chromosomes. Wilcoxon tests show significant differences in K_a/K_s ratios between neo-X versus neo-Y genes, genes with intact neo-Y copies with versus without expression ($P = 0.000242$), and disrupted versus intact transcribed neo-Y genes ($P = 2.971 \times 10^{-12}$). Different levels of significance are marked as asterisks. (**D**) The frequency distribution of K_a/K_s ratios of neo-X and neo-Y genes.

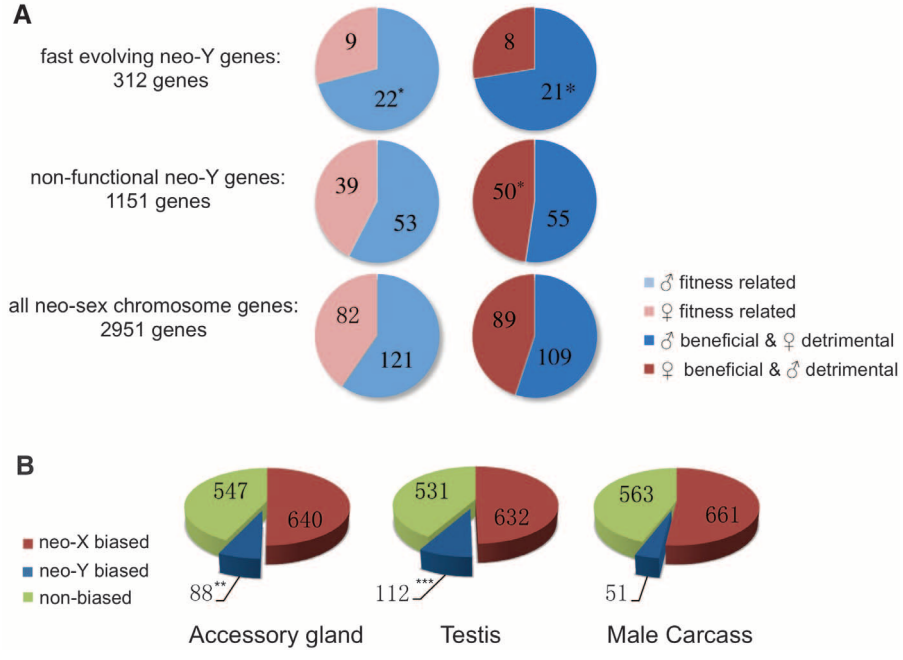

Fig. 3. (**A**) Sex-specific fitness effects and sexual antagonism of neo-sex genes (light blue, male-fitness related; light red, female-fitness related; dark blue, male-beneficial/female-detrimental; dark red, female-beneficial/male-detrimental). Significance is evaluated by comparing all neo-sex genes to either fast evolving or nonfunctional neo-Y genes (*$P < 0.05$, **$P < 0.01$). (**B**) The number of neo-X–biased (red), neo-Y–biased (blue), and nonbiased (green) genes in different tissues of male *D. miranda*.

various gene ontology (GO) categories of primary metabolic processes (such as GO 0046165, 0016042, and 0006094), whereas genes involved in regulatory (GO 0050789 and 0048519) or developmental processes (GO 0032502) tend to maintain nonbiased expression and intact ORFs (one-tailed Fisher's exact test, $P < 0.01$) (tables S5 and S6). Thus, although natural selection is impaired on the neo-Y, it tends to maintain haploinsufficient genes (such as regulatory genes), whereas haplosufficient genes (such as metabolic enzymes) are more prone to degeneration (*18*). Overall, ~40% of the neo-Y genes have lost their functions within 1 million years.

Deleterious mutations with more subtle effects also accumulate on the neo-Y. We calculated pairwise rates of nonsynonymous (K_a) and synonymous changes (K_s), and their ratios (ω), using *D. pseudoobscura* as an outgroup. Genes on the neo-Y evolve significantly faster than do their neo-X homologs or genes on other chromosomes at both synonymous and nonsynonymous sites (Wilcoxon test, $P < 0.01$) (table S7). Selection to maintain codon usage bias is reduced in *D. miranda* (*19*); thus, patterns of synonymous changes (K_s) should largely reflect mutational differences. Although neo-Y genes generally show lower codon bias (table S7), this difference is not statistically significant between

the neo-X and neo-Y or between functional and nonfunctional neo-Y genes (Wilcoxon test, $P > 0.05$). Thus, the contribution of codon bias selection to elevated K_s patterns appears limited and instead may reflect male-driven evolution (*20*). Neo-Y genes with disrupted ORFs evolve significantly faster at the protein level than do those with intact ORFs (Wilcoxon test, $P = 2.97 \times 10^{-12}$) (Fig. 2C), and intact but silenced neo-Y genes evolve significantly faster than do those still expressed from the neo-Y (Wilcoxon test, $P = 2.42 \times 10^{-4}$) (Fig. 2C). This suggests that neo-Y genes with disrupted ORFs or silenced expression are subject to little selective constraint, and we classified all these genes as nonfunctional in subsequent analysis (fig. S4) (*17*). The distribution of ω at neo-Y genes is shifted toward neutral evolution ($\omega = 1$), and the proportion of genes under strong selective constraints ($\omega < 0.1$) is greatly reduced as compared with neo-X genes (15.02 versus 38.78%) (Fig. 2D). This pattern is consistent with an accumulation of mildly deleterious amino acid mutations at many neo-Y loci.

Decay in gene function is the primary but not only force driving early Y evolution. Y chromosomes are limited to males, and genes found on ancient Ys often have male-specific function (*3*, *4*). It is unclear whether male-related genes only accumulate on old, gene-poor Ys, where adaptive mutations experience little interference from segregating deleterious mutations, or whether masculinization accompanies early stages of Y evolution, and thus contributes to degeneration through hitchhiking effects (fixations of deleterious mutations linked to strongly beneficial alleles) (*2*). To explore whether adaptive evolution for male-function is operating on neo-Y genes, we performed maximum-likelihood analysis of the lineage-specific ω ratio of all functional neo-sex genes (*17*). We identified 312 transcribed genes evolving significantly faster on the neo-Y lineage (as compared with 66 genes evolving faster on the neo-X lineage; likelihood ratio test, $P < 0.05$) and evaluated whether this set of functional neo-Y genes shows characteristics of male-specific selection. Recently acquired male-limited inheritance releases sexually antagonistic male-beneficial/female-detrimental mutations from counter selection in females, and such genes may show increased rates of adaptive evolution on the neo-Y. We classified orthologous *D. miranda* genes according to a sexual antagonism scheme proposed for *D. melanogaster* (table S8) (*21*) and found a significant enrichment of male-beneficial/female-detrimental genes or genes correlated with male-specific fitness among the fast-evolving neo-Y genes (Fisher's exact test, $P < 0.05$) (Fig. 3A). These gene categories are not enriched among nonfunctional genes, indicating that male-beneficial genes are under selective constraint on the neo-Y and that male-specific selection is driving adaptive protein evolution at some neo-Y genes. Genes related to male fitness are more likely to be functional on the neo-Y, whereas genes classified as female-beneficial/male-detrimental are enriched for genes with disrupted ORFs or silenced expression (Fig. 3A). This suggests that although selection operates to maintain male-beneficial genes, those harming males are actively removed from the neo-Y. Transcriptome analysis of male-specific organs (testis and accessory gland) versus male somatic carcass tissues (removing these organs) provides additional evidence for masculinization. In all tissues, the majority of genes show neo-X–biased expression. However, testis and accessory glands harbor about twice as many genes with neo-Y–biased expression as compared with that of male somatic carcass (Fisher's exact test, $P < 0.05$) (Fig. 3B), caused by up-regulation of the neo-Y alleles (fig. S5) (*17*). Also, functional neo-Y genes in *D. miranda* have evolved significantly increased expression-specificity in accessory glands (relative to male somatic carcass tissues) as compared with that of their orthologous *D. pseudoobscura* genes (figs. S6 and S7) (*17*). Further, genes with significant neo-Y–biased expression are enriched for male reproductive GO terms, including "insemination," "copulation," and "reproductive process" (GO 0007320, 0007620, and 0022414) (table S11). Thus, although most neo-Y genes undergo degeneration, a subset acquires or improves male-related functions. The absence of sexual conflicts on a male-limited chromosome enables male-specific adaptation and may appreciably contribute to Y degeneration through the hitchhiking effect (*22*).

Evolutionary forces on an evolving X chromosome can operate in opposite directions. Female-biased transmission will favor female-specific genes and disfavor male-beneficial genes. Old X chromosomes in *Drosophila* contain a deficiency of genes expressed in male-specific tissue (*5*, *6*). In *D. miranda*, both chrXL and chrXR show a clear under-representation of testis and accessory gland genes (Fisher's exact test, $P < 0.05$) (Fig. 4A), and ovary expression is higher for genes located on chrXL and chrXR (Wilcoxon test, $P < 0.05$) (Fig. 4B) (*17*). Thus, an X chromosome becomes fully demasculinized and feminized within 10 to 18 million years in *Drosophila* (*5*). No chromosome-wide changes in overall expression patterns in sex tissues are observed on the neo-X (Fig. 4, A and B), and its origin may be too recent for a large turnover of gene content to have taken place. Young X-linked genes in *Drosophila* tend to be male-biased (*23*), possibly because of the fixation of recessive, male-beneficial mutations, and demasculinization appears to happen over longer evolutionary time periods. In *D. miranda*, approximately half of the neo-X genes have no functional neo-Y homologs (they are hemizygous) and might show different evolutionary dynamics than those with functional neo-Y copies (diploid neo-X genes). We find that hemizygous genes evolve significantly faster at their neo-X branch than do diploid ones (median ω ratios of 0.1416 versus 0.0997, Wilcoxon test, $P = 0.0005187$) (Fig. 4C). If male-beneficial

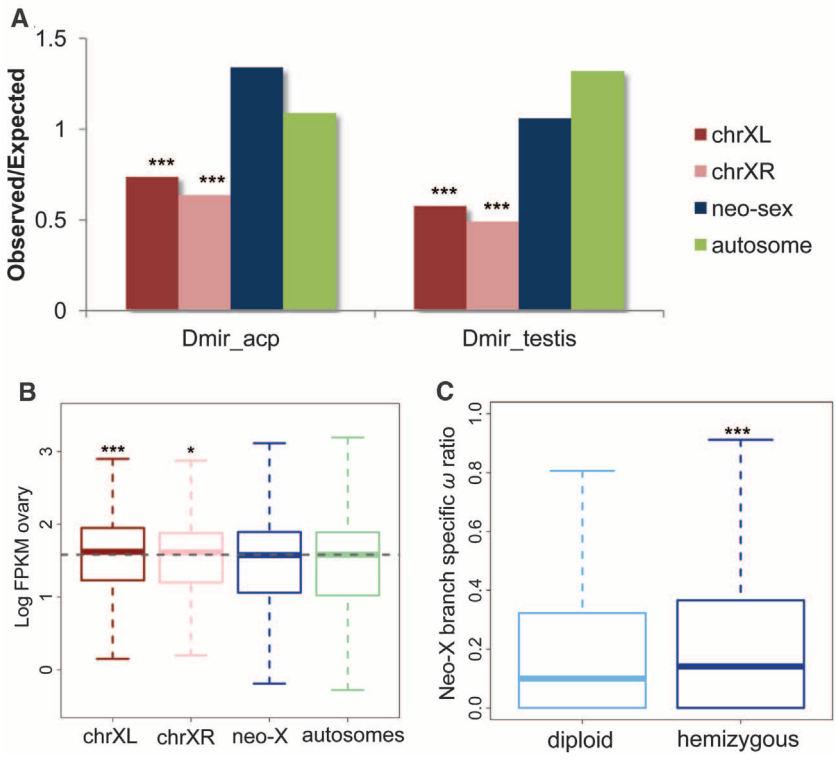

Fig. 4. (**A**) The observed/expected ratio of genes highly expressed (top 500; fig. S7 for different cutoffs) in testis or accessory glands. (**B**) Log-based absolute expression levels [fragments per kilobase of exon per million fragments mapped (FPKM)] from ovary for each chromosome (fig. S7). (**C**) The ω ratio on the neo-X branch at hemizygous and diploid neo-X genes.

adaptation drives elevated protein evolution at hemizygous neo-X genes, this pattern should be more pronounced for genes expressed highly in a male-specific tissue. Indeed, hemizygous (but not diploid) neo-X genes show a significant positive correlation between their absolute expression levels in accessory gland and ω ratios (F-statistic comparing diploid versus hemizygous neo-X genes, $P < 0.05$) (*17*), and a similar trend is observed for expression levels in testis but not somatic genes (fig. S11) (*17*). Thus, masculinization occurs on hemizygous neo-X loci, whereas demasculinization and feminization dominate on chrXL and chrXR. Gene loss, gain, and movement appear as the dominant mechanisms for depleting male genes on the X (*5*), and differences in dominance and rates could contribute to the observed temporal dynamics of masculinization and feminization/demasculinization. Recessive male-beneficial amino acid substitutions might accumulate relatively quickly in hemizgyous neo-X genes, whereas gene content turnover removing male genes might proceed slowly over longer time periods. Also, demasculinization might result from cellular processes that only operate on older X chromosomes, such as dosage compensation or silencing of the X during spermatogenesis (*24*, *25*). Overall, a variety of—and sometimes opposing—evolutionary forces operate on evolving sex chromosomes because of common sexual conflicts.

References and Notes

1. J. J. Bull, *Evolution of Sex Determining Mechanisms* (Benjamin Cummings, Menlo Park, CA, 1983).
2. B. Charlesworth, D. Charlesworth, *Philos. Trans. R. Soc. Lond. B Biol. Sci.* **355**, 1563 (2000).
3. L. B. Koerich, X. Wang, A. G. Clark, A. B. Carvalho, *Nature* **456**, 949 (2008).
4. H. Skaletsky *et al.*, *Nature* **423**, 825 (2003).
5. D. Sturgill, Y. Zhang, M. Parisi, B. Oliver, *Nature* **450**, 238 (2007).
6. E. Betrán, K. Thornton, M. Long, *Genome Res.* **12**, 1854 (2002).
7. B. Charlesworth, J. Coyne, N. Barton, *Am. Nat.* **130**, 113 (1987).
8. B. Vicoso, B. Charlesworth, *Nat. Rev. Genet.* **7**, 645 (2006).
9. H. J. Muller, in *The New Systematics*, J. Huxley, Ed. (Clarendon Press, Oxford, 1940), pp. 185–268.
10. M. Steinemann, S. Steinemann, *Genetica* **102/103**, 409 (1998).
11. A. B. Carvalho, A. G. Clark, *Science* **307**, 108 (2005).
12. I. Marín, A. Franke, G. J. Bashaw, B. S. Baker, *Nature* **383**, 160 (1996).
13. D. Bachtrog, B. Charlesworth, *Nature* **416**, 323 (2002).
14. M. Steinemann, S. Steinemann, F. Lottspeich, *Proc. Natl. Acad. Sci. U.S.A.* **90**, 5737 (1993).
15. D. Bachtrog, *Nat. Genet.* **34**, 215 (2003).
16. D. Bachtrog, E. Hom, K. M. Wong, X. Maside, P. de Jong, *Genome Biol.* **9**, R30 (2008).
17. Materials and methods are available as supplementary materials on *Science* Online.
18. F. A. Kondrashov, E. V. Koonin, *Trends Genet.* **20**, 287 (2004).
19. D. Bachtrog, *Genetics* **165**, 1221 (2003).
20. D. Bachtrog, *Mol. Biol. Evol.* **25**, 617 (2008).
21. P. Innocenti, E. H. Morrow, *PLoS Biol.* **8**, e1000335 (2010).
22. D. Bachtrog, *Nat. Genet.* **36**, 518 (2004).
23. Y. E. Zhang, M. D. Vibranovski, B. H. Krinsky, M. Long, *Genome Res.* **20**, 1526 (2010).
24. D. Bachtrog, N. R. Toda, S. Lockton, *Curr. Biol.* **20**, 1476 (2010).
25. E. Lifschytz, D. L. Lindsley, *Proc. Natl. Acad. Sci. U.S.A.* **69**, 182 (1972).

Acknowledgments: We thank R. Nielsen, M. Eisen, X. Xun, and L. Tian for help and discussion. This work was funded by NIH grants (R01GM076007 and R01GM093182) and a Packard Fellowship to D.B. All DNA/RNA-seq reads are deposited at www.ncbi.nlm.nih.gov/sra under accession no. SRA048115. The genome assembly and annotation is available at the National Center for Biotechnology Information under BioProject ID PRJNA77213.

Supplementary Materials

www.sciencemag.org/cgi/content/full/337/6092/341/DC1
Materials and Methods
Figs. S1 to S11
Tables S1 to S12
References (*26*–*44*)

30 May 2012; accepted 7 June 2012
10.1126/science.1225385

Hypoxia Triggers Meiotic Fate Acquisition in Maize

Timothy Kelliher* and Virginia Walbot*

Evidence from confocal microscopic reconstruction of maize anther development in fertile, *mac1* (excess germ cells), and *msca1* (no germ cells) flowers indicates that the male germ line is multiclonal and uses the MAC1 protein to organize the somatic niche. Furthermore, we identified redox status as a determinant of germ cell fate, defining a mechanism distinct from the animal germ cell lineage. Decreasing oxygen or H_2O_2 increases germ cell numbers, stimulates superficial germ cell formation, and rescues germinal differentiation in *msca1* flowers. Conversely, oxidizing environments inhibit germ cell specification and cause ectopic differentiation in deeper tissues. We propose that hypoxia, arising naturally within growing anther tissue, acts as a positional cue to set germ cell fate.

Most animals sequester germline stem cells during embryogenesis (*1*, *2*), whereas plants are strictly vegetative until intrinsic and environmental cues trigger reproduction (*3*, *4*). The morphogenetic mechanism underlying the somatic-to-germinal switch is a botanical mystery, which if understood would permit tailored manipulations in crop breeding and yield enhancement.

The angiosperm male germ line develops in immature anthers, within each of four lobes surrounding a central vasculature (*5*), viewed transversely as a butterfly shape (fig. S1). We tracked cellular ontogeny in three-dimensional reconstructions of ~1000 fertile anthers by confocal microscopy, finding that anther length is a precise and reliable proxy for developmental stage. In 70- to 120-μm-long anthers, each lobe consisted of 15 to 20 isodiametric L2-d (layer 2–derived, tracing back to the second meristem layer) cells, haphazardly arranged with 3 to 5 cells in transverse view (fig. S2). Starting at 120 μm and continuing for 30 hours to ~220 μm, successive, symmetric divisions in different L2-d progenitors yielded a column of 8 to 12 presumptive germinal cells, initiating centrally where lobes are widest and completing at the tapered tip and base (Fig. 1A and figs. S3 and S4). The majority of these presumptive archesporial cells derived from apical progenitors [63%, 67 out of 106 (67/106)], but 21% were lateral (22/106), and 16% were basal (17/106) (Fig. 1B). Therefore, in a fertile lobe, all L2-d cells can generate presumptive archesporial cells, which are central in transverse view, surrounded by four or five L2-d neighbors. Initially these presumptive germ cells lacked the well-established (*6*) morphological traits of premeiotic cells, but ~12 hours after birth, archesporial cells were distinguished from neighboring L2-d cells by their enlarged and nonrectilinear shape, dimly mottled cytoplasmic stain, and 2-μm-wide unstained boundary. Differentiated archesporial cells contained elevated amounts of MAC1 protein, a molecular marker for fate acquisition (Fig. 1C) (*7*).

Shortly after archesporial cell enlargement in the transverse view, encircling L2-d cells began dividing periclinally, founding the secondary parietal layer and endothecium. This process begins centrally at ~180 μm, and a full somatic bilayer is constituted by ~280 μm. In *multiple archesporial cells 1* (*mac1*) male sterile anthers, the bilayer is replaced by a single faulty layer and excess archesporial cells (*8*). In primordia (<120-μm anther length) and later developmental stages, *mac1* lobes had extra L2-d cells, including supernumerary central cells, all of which differentiated as archesporial (Fig. 1A and fig. S5). The encircling ring of L2-d cells generated additional archesporial cells for 24 hours after normal cessation (Fig. 1, A and D), never forming the somatic bilayer. Once specified, *mac1* archesporial cells proliferated excessively: 30% were EdU+ (5'-ethynyl-2'-deoxyuridine) versus 12% in fertile anthers (fig. S6). When analyzed by quantitative real-time polymerase chain reaction (qRT-PCR), *Mac1* transcripts were low in anther primordia; expression increased 20-fold during germinal specification (anther length, 150 μm) and was highly specific to laser-microdissected archesporial cells both 1 and 3 days after

Department of Biology, Stanford University, Stanford, CA 94305, USA.

*E-mail: tkellih1@stanford.edu (T.K.); walbot@stanford.edu (V.W.)

Science

Sex-Specific Adaptation Drives Early Sex Chromosome Evolution in *Drosophila*

Qi Zhou and Doris Bachtrog

Science **337** (6092), 341-345.
DOI: 10.1126/science.1225385

Sex Chromosome Evolution

The fly genus *Drosophilia* has repeatedly generated evolutionarily new sex chromosomes. To understand the changes shaping the X and Y chromosomes, **Zhou and Bachtrog** (p. 341), sequenced the genome of *D. miranda*, which formed neo-X and neo-Y chromosomes approximately 1 million years ago. The data illuminate the ongoing conflict between selection for male and female function on the sex chromosomes and show that Y chromosome evolution is characterized both by a loss of gene function and selection for male-specific adaptations in genes beneficial to male functions.

Science (print ISSN 0036-8075; online ISSN 1095-9203) is published by the American Association for the Advancement of Science, 1200 New York Avenue NW, Washington, DC 20005. The title *Science* is a registered trademark of AAAS.